Therapeutic Potential of ^{90}Y- and ^{131}I-Labeled Anti-CD20 Monoclonal Antibody in Treating Non-Hodgkin's Lymphoma with Pulmonary Involvement: A Monte Carlo–Based Dosimetric Analysis

Hong Song[1], Yong Du[2], George Sgouros[1], Andrew Prideaux[1], Eric Frey[2], and Richard L. Wahl[1]

[1]*Division of Nuclear Medicine, Russell H. Morgan Department of Radiology and Radiological Science, School of Medicine, Johns Hopkins University, Baltimore, Maryland; and* [2]*Division of Medical Imaging Physics, Russell H. Morgan Department of Radiology and Radiological Science, School of Medicine, Johns Hopkins University, Baltimore, Maryland*

Pulmonary involvement is common in patients with non-Hodgkin's lymphoma (NHL). ^{90}Y- and ^{131}I-anti-CD20 antibodies (ibritumomab tiuxetan and tositumomab, respectively) have been approved for the treatment of refractory low-grade follicular NHL. In this work, we used Monte Carlo–based dosimetry to compare the potential of ^{90}Y and ^{131}I, based purely on their emission properties, in targeted therapy for NHL lung metastases of various nodule sizes and tumor burdens. **Methods:** Lung metastases were simulated as spheres, with radii ranging from 0.2 to 5.0 cm, which were randomly distributed in a voxelized adult male lung phantom. Total tumor burden was varied from 0.2 to 1,641 g. Tumor uptake and retention kinetics of the 2 radionuclides were assumed equivalent; a uniform distribution of activity within tumors was assumed. Absorbed dose to tumors and lung parenchyma per unit activity in lung tumors was calculated by a Monte Carlo–based system using the MCNP4B package. Therapeutic efficacy was defined as the ratio of mean absorbed dose in the tumor to that in normal lung. Dosimetric analysis was also performed for a lung-surface distribution of tumor nodules mimicking pleural metastatic disease. **Results:** The therapeutic efficacy of both ^{90}Y and ^{131}I declined with increasing tumor burden. In treating tumors with radii less than 2.0 cm, ^{131}I targeting was more efficacious than ^{90}Y targeting. ^{90}Y yielded a broader distribution of tumor absorbed doses, with the minimum 54.1% lower than the average dose; for ^{131}I, the minimum absorbed dose was 33.3% lower than the average. The absorbed dose to normal lungs was reduced when the tumors were distributed on the lung surface. For surface tumors, the reductions in normal-lung absorbed dose were greater for ^{90}Y than for ^{131}I, but ^{131}I continued to provide a greater therapeutic ratio across different tumor burdens and sizes. **Conclusion:** Monte Carlo–based dosimetry was performed to compare the therapeutic potential of ^{90}Y and ^{131}I targeting of lung metastases in NHL patients. ^{131}I provided a therapeutic advantage over ^{90}Y, especially in tumors with radii less than 2.0 cm and at lower tumor burdens. For both ^{90}Y- and ^{131}I-labeled antibodies, treatment is more efficacious when applied to metastatic NHL cases with lower tumor burdens. ^{131}I has advantages over ^{90}Y in treating smaller lung metastases.

Key Words: non-Hodgkin's lymphoma; pulmonary metastases; dosimetry; Monte Carlo; ^{90}Y; ^{131}I

J Nucl Med 2007; 48:150–157

Intrathoracic involvement is common in non-Hodgkin's lymphoma (NHL). Pulmonary involvement is found in about 24% of NHL patients (*1,2*). Chylothorax due to lymphatic obstruction and leakage leads to pleural effusion, which is usually associated with widely disseminated disease and a poor prognosis (*1*). Many NHL patients will relapse after treatment, and previously indolent lymphomas can transform into a more aggressive histologic type. Once transformation occurs, NHL becomes highly refractory to most conventional therapies (*3,4*). Radioimmunotherapy, using anti-CD20 antibodies, has been approved as a new treatment modality for NHL. Both ^{90}Y-labeled antibodies (Zevalin [ibritumomab tiuxetan]; IDEC Pharmaceuticals) and ^{131}I-labeled antibodies (Bexxar [tositumomab]; GlaxoSmithKline) have shown good therapeutic efficacy for patients with relapsed or refractory low-grade follicular NHL (*4–9*). Both radioimmunoconjugates have been investigated with autologous hematopoietic stem cell transplantation and in combination with chemotherapy (*10–14*). In this setting, the lung was the dose-limiting organ, with a maximum tolerated dose of 27 Gy for ^{131}I-tositumomab (*10,12,15*). In trials with myeloablative ^{90}Y-ibritumomab tiuxetan, the dose-limiting organ was less well established, with normal organs receiving a target dose of 10 Gy (*14*). With both

Received Jun. 8, 2006; revision accepted Sep. 13, 2006.

For correspondence or reprints contact: George Sgouros, PhD, CRB II 4M.61, 1550 Orleans St., Johns Hopkins University, School of Medicine, Baltimore, MD 21231.

E-mail: gsgouros@jhmi.edu

agents, the high-dose, myeloablative approach showed promising efficacy, especially when combined with chemotherapy (*10,12*).

Although both ^{90}Y-ibritumomab tiuxetan and ^{131}I-tositumomab have produced a good overall response in the treatment of low-grade refractory or relapsed transformed NHL, they are different in their pharmacokinetics and *in vivo* stability. Most importantly, the conjugated radionuclide ^{90}Y is a pure β-emitter with an average energy of 935 keV and a half-life of 64 h, whereas ^{131}I emits both β-rays with an average energy of 183 keV and γ-rays with a half-life of 192.5 h (Table 1). The physical properties of the 2 radioisotopes are a critical parameter in the choice of the 2 anti-CD20 radioimmunoconjugates. The putative advantages of ^{90}Y in tumor targeting are its higher energy and longer pathlength (0.25 cm), which make it suitable for treating NHL tumors with diameters larger than 1.0 cm or with necrotic cores that require a cross-fire effect in order to be sterilized, whereas ^{131}I is more suitable for targeting micrometastases (*16*). The higher doses delivered by ^{90}Y to normal organs, however, limits the radioactivity that may be administered for therapy.

The presence of pulmonary metastases in NHL patients increases the dose absorbed by normal lungs, thus limiting the prescribed treatment activity. Accurate calculation of lung absorbed dose is difficult with the conventional whole-organ S value–based dosimetry or point-kernel approaches when disseminated tumor nodules are in the lungs (*17*). The low density of lung tissue invalidates the assumption that electron energy will be locally deposited, and disseminated disease leads to a heterogeneous tissue composition, coupled with a nonuniform activity distribution, thereby complicating the dose calculation. Monte Carlo–based dosimetry is better suited for such cases.

In this work, we used Monte Carlo–based dosimetry to compare the potential of ^{90}Y and ^{131}I, based purely on their emission properties, in labeled monoclonal antibody treatment of NHL lung metastases of various nodule sizes and tumor burdens. Assuming that the lungs are the dose-limiting organ in the myeloablative setting, the absorbed dose delivered to normal lung tissue served as the basis for comparing therapeutic efficacy.

TABLE 1
Physical Properties of ^{90}Y and ^{131}I

Isotope	Half-life (h)	Radiation type	Energy (keV)	Mean range (cm)
^{90}Y	64	β	935/2,280	0.25
^{131}I	192.5	β	183/807	0.04
		γ	378/364 (81.7%)	

Data were obtained from Lund/LBNL Nuclear Data Search. β-Energy is presented as mean/maximum. γ-Energy is presented as mean/most abundant (abundance).

MATERIALS AND METHODS

To investigate the relative efficacy of ^{90}Y and ^{131}I in the targeted therapy of lung metastases, we estimated the absorbed dose to simulated lung tumors and to normal lung parenchyma using Monte Carlo–based dosimetry. A voxelized representation of the Cristy–Eckerman adult male lung phantom was used as the normal-lung model into which tumor nodules were placed to simulate lung metastases (*18*). The comparison was based on the therapeutic ratio, defined as the absorbed dose to tumor divided by the absorbed dose to normal lung parenchyma.

Lung Phantom

Every voxel whose center lay within the surface of the lungs was included as part of the phantom. The lung phantom thus generated contained 52,700 voxels of $4 \times 4 \times 4$ mm within a $72 \times 64 \times 48$ voxel cube (Figs. 1A–1C). A 4-mm voxel size was chosen because it is a common voxel size in SPECT and PET. The mass of the voxelized lung phantom was 998 g, about 0.2% lower than that of the Cristy–Eckerman lung phantom. This phantom was then converted into the appropriate Monte Carlo code input format for dose calculation.

Monte Carlo Code

The MCNP4B Monte Carlo code (Oak Ridge National Laboratory) was used to perform the dosimetry calculations (*19*). The Monte Carlo methodology developed for lung dosimetry using this code, as well as its validation, has previously been described (*17*). The full photon and electron spectrums of ^{131}I and ^{90}Y were obtained from The Lund/LBNL Nuclear Data Search (version 2.0, 1999; http://nucleardata.nuclear.lu.se/nucleardata/toi/) (*20*). For all cases, a sufficient number of electron and photon transport histories were generated to produce statistically reliable energy tallies, with relative errors less than 0.10. Validation involved

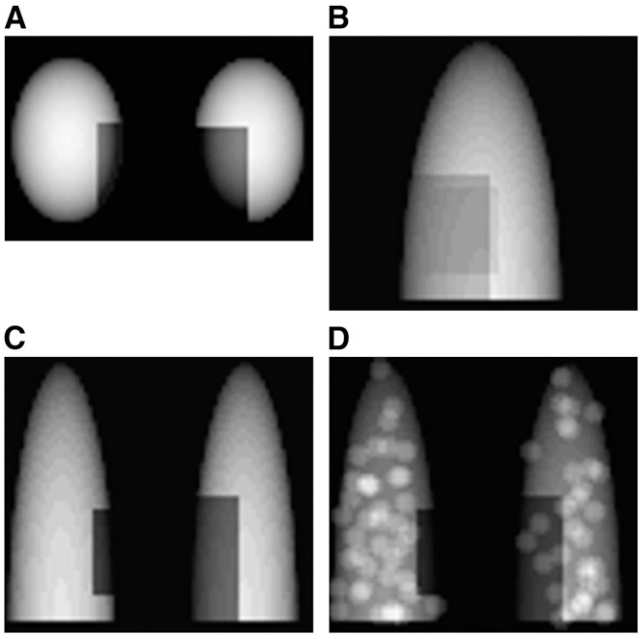

FIGURE 1. (A–C) Voxelized Cristy-Eckerman lung phantom shown in transverse (A), coronal (B), and sagittal (C) projection views. (D) Coronal projection view of 72 randomly distributed tumors of 1.0-cm radius in voxelized lung phantom.

reproducing the ^{131}I lung-to-lung S values found in OLINDA. The calculation was repeated for ^{90}Y. The lung-to-lung self-absorbed doses for ^{131}I and ^{90}Y were about 6.0% lower and 13.4% lower, respectively, than those obtained from the OLINDA software package (*21*). The differences are likely explained by the fact that, in the MCNP4B package, electrons are assumed not to be deposited locally but to be transported explicitly.

Impact of Density on Self-Dose and Cross Dose

To examine the impact of density differences and β-particle emission energy on electron transport for ^{90}Y relative to ^{131}I, we calculated the energy deposition by electrons from ^{131}I and ^{90}Y in spheres with densities of 1.0 or 0.296 g/cm^3. Spheres with radii of 50 μm to 5.0 cm were filled with water at a density of 1.0 g/cm^3 or lung tissue at a density of 0.296 g/cm^3. Activity was uniformly distributed within the spheres.

When tumors are present in the lung tissue, explicitly transported electrons are able to reach nearby tumors or normal lung tissues, delivering to tumors or normal tissues "cross-fire" doses with a pure β-emitter such as ^{90}Y. To demonstrate this effect, we simulated a simplified scenario in which 2 spheres—a source sphere and a target sphere—of the same radius were filled with water and placed side by side in direct contact with each other. They were surrounded by either water or lung tissue. Activity was uniformly distributed in the source sphere, and the fraction of electron energy deposited in the neighboring target sphere was calculated when both sphere radii were varied simultaneously.

Therapeutic Efficacy of Tumors in Lungs

The therapeutic efficacy of ^{90}Y- and ^{131}I-labeled antibody in targeting different sizes of tumors at various tumor burdens was evaluated. The densities of tumor and normal lung tissue are 1.04 and 0.2958 g/cm^3, respectively, in all subsequent calculations. Therapeutic efficacy was defined as the absorbed dose to tumors per unit of tumor-cumulated activity (mGy/MBq-s) divided by the absorbed dose to normal lungs per unit of tumor-cumulated activity (mGy/MBq-s). A series of phantoms were generated. Each phantom contained a uniformly distributed set of randomly placed computer-generated tumors of the same radius. Tumor radii ranged from 0.2 to 5.0 cm. None of the tumors overlapped. An example projection image of a lung phantom containing 72 tumors with a radius of 1 cm is shown in Figure 1D. A tumor with a radius of 1.0 cm on average consists of 81 voxels of $4 \times 4 \times 4$ mm each. A tumor burden range of about 0.2–1,641 g, for each tumor size, was achieved by changing the number of tumors. Activity was assumed to be uniformly distributed in the tumors only, and no activity was assigned to normal lungs. Differences in pharmacokinetics and nonuniform antibody penetration in tumor nodules were not evaluated, nor were the possible differences in the fate of the radionuclide after radioantibody internalization. Nontumor voxels were designated as normal lung tissues. The specific absorbed dose to both tumors and lungs was then calculated after MCNP4B electron and photon transport for every tumor size and tumor burden. Therapeutic efficacies for both ^{90}Y and ^{131}I were calculated and compared.

A nonuniform absorbed dose distribution in tumors and lungs could compromise the dose response in tumors. The spatial distribution of absorbed dose was obtained for 1-cm tumor nodules randomly distributed throughout the lungs and a tumor burden of 5.4 g. The spatial distribution of absorbed dose by ^{131}I and ^{90}Y in both tumor and normal lung was represented using dose-volume histograms. The effects of a nonuniform dose distribution in the tumors were not investigated.

Surface-Distributed Tumors

The spatial distribution of tumor nodules within the lungs may considerably affect the absorbed dose to lungs and also to tumor. To examine this effect, we performed a dosimetric analysis with the centers of the tumors placed on the lung surfaces. The same radius and tumor burden distribution were used except that all the tumors were now randomly and uniformly distributed on the lung surfaces. For both ^{90}Y and ^{131}I, the absorbed dose to normal lungs was compared with that obtained when tumors were uniformly distributed throughout the lungs.

RESULTS

The impact of normal lung density on energy deposition by electrons is shown in Figure 2. Spheres of lung density absorbed a smaller fraction of electron energy both for ^{131}I

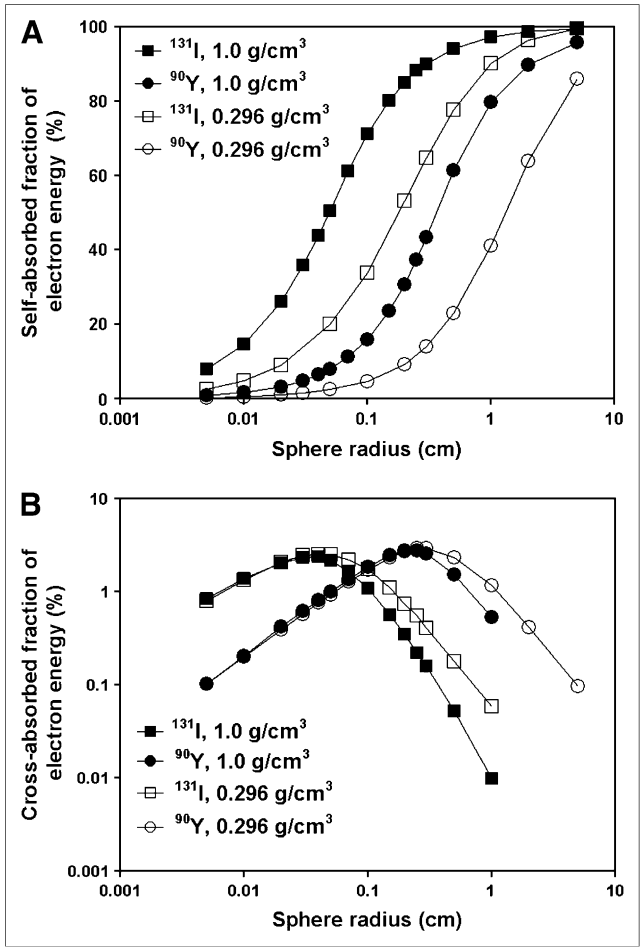

FIGURE 2. (A) Absorbed fraction of electron energy deposited in spheres with radii ranging from 50 μm to 5.0 cm. Spheres were filled with water (density of 1.0 g/cm^3) or lung tissue (density of 0.296 g/cm^3) and uniformly distributed with ^{90}Y or ^{131}I. (B) Absorbed fraction of electron energy deposited in neighboring target sphere by ^{90}Y or ^{131}I. Both source and target sphere were filled with water. They were surrounded by either water or lung tissue. Solid symbols indicate water-filled spheres; open symbols indicate lung-tissue–filled spheres.

and for ^{90}Y (Fig. 2A). The fraction of energy absorbed in spheres of radius 1.0 cm decreased from 97.3% to 90.2% for ^{131}I and from 79.8% to 41.2% for ^{90}Y. When tumors were surrounded by normal lung tissue, both ^{131}I and ^{90}Y electrons were able to deliver more cross-fire doses to the target sphere (Fig. 2B). Electrons from ^{90}Y, because of their higher mean energy, have a longer mean range in both water and lung tissue than do electrons from ^{131}I. For spheres with a 1.0-cm radius, the fraction of electron energy absorbed in the target sphere was 1.2% for ^{90}Y, compared with 0.1% for ^{131}I. The fraction of electron energy absorbed in the target sphere increased with increasing target sphere size but decreased with increasing source sphere radius. The maximum absorbed energy fraction (2.54% for ^{131}I and 2.94% for ^{90}Y) in the target sphere was reached at 0.04 cm for ^{131}I and 0.25 cm for ^{90}Y when the radii of both source and target sphere were the same.

The therapeutic efficacies of both ^{131}I and ^{90}Y declined as tumor burden increased. This reduction occurred regardless of tumor nodule size (Figs. 3A and 3B). For example, for tumors 1.0 cm in radius, the therapeutic efficacy ratio dropped from 720.3 to 2.8 for ^{90}Y and from 1,607.9 to 6.1 for ^{131}I when the tumor burden was increased from 5.4 to 1,552.7 g. This sharp deterioration can be attributed mainly to the increase in lung dose when activity concentration remains constant for larger tumor burdens. Therapeutic efficacy, however, was better for larger-diameter tumors at a constant tumor burden. This improvement was more evident when using ^{90}Y than when using ^{131}I. At a tumor burden that was approximately 12% of the total lung mass, the therapeutic efficacy for 2.0-cm tumors improved relative to that for 0.2-cm tumors by a factor of 6.1 with ^{90}Y but only 2.2-fold with ^{131}I. This difference in efficacy as a function of tumor size for the 2 isotopes is caused by the fact that ^{90}Y is a pure β-emitter and, thus, that tumor absorbed energy is largely determined by tumor size. ^{131}I also emits photons, the energy deposition of which, however, is less sensitive to tumor size.

As shown in Figure 3C, the therapeutic efficacy of ^{131}I was greater than that of ^{90}Y across all tumor nodule sizes and tumor burdens considered. The therapeutic ratio calculated for ^{131}I was 6.0 times higher than that for ^{90}Y when tumor radius was 0.2 cm and tumor burden was 0.2 g; the ratio was 3.0 when total tumor burden was 859.6 g. This decline can be attributed in part to an increased tumor dose from ^{90}Y at a higher tumor burden because of the cross-fire effects. Although electron energy is usually assumed to be deposited locally, for ^{90}Y electrons of an average 935 keV, electron energy could still reach neighboring tumors in low-density lung tissue. For larger tumors, the therapeutic advantage of ^{131}I over ^{90}Y decreased. When tumor radius reached 2.0 cm, both ^{131}I and ^{90}Y yielded therapeutic efficacy ratios of 1.4. For 5.0-cm tumors, the therapeutic efficacy for ^{131}I was about 30% smaller than that for ^{90}Y. The indicated tumor burden range does not seem to affect the therapeutic efficacy ratio between ^{131}I and ^{90}Y for tumors with radii larger than 1.0 cm. As shown in Figure 2B, this is most likely because the cross-fire dose to adjacent tumor nodules decreased with increasing tumor size.

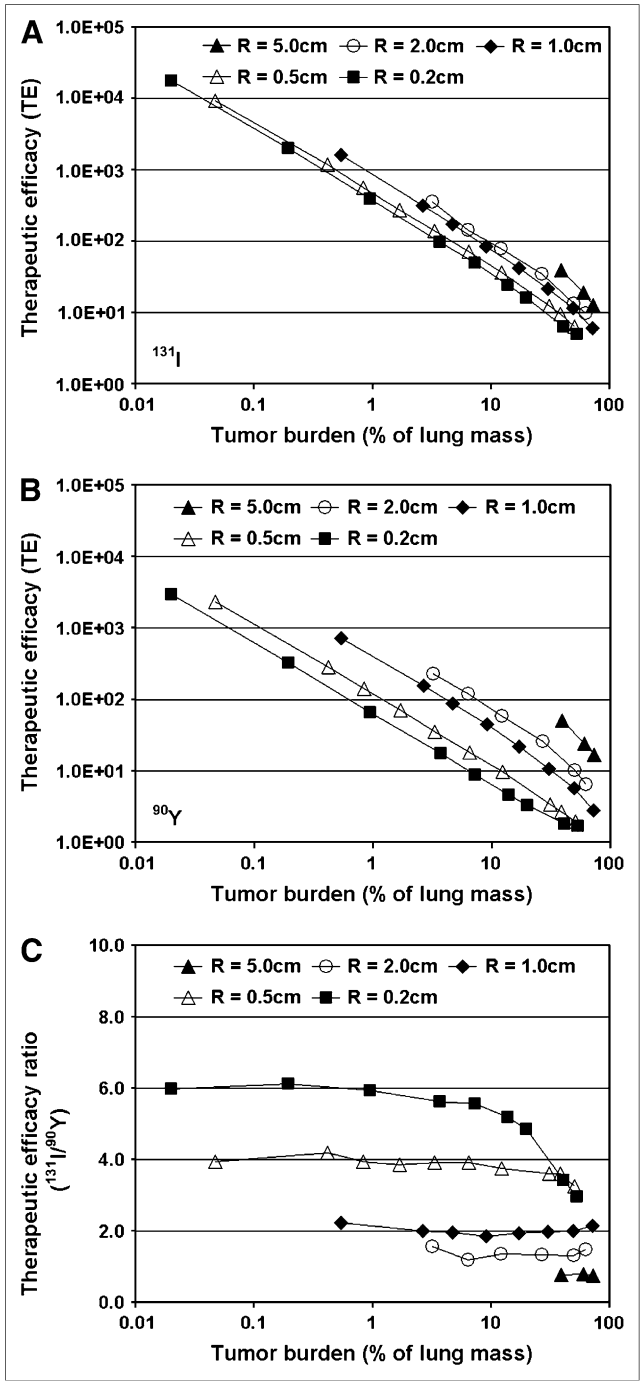

FIGURE 3. (A and B) Therapeutic efficacy of ^{131}I (A) and ^{90}Y (B) in treating tumor nodules in lungs. Tumors with radii ranging from 0.2 to 5.0 cm were randomly and uniformly distributed in lungs. Total tumor burden was varied from 0.2 to 1,641 g by varying the number of tumors. (C) Therapeutic efficacy ratio of ^{131}I to ^{90}Y for various tumor sizes and tumor burdens.

The dose–volume histograms of absorbed dose within tumors and normal lungs are shown in Figure 4. With

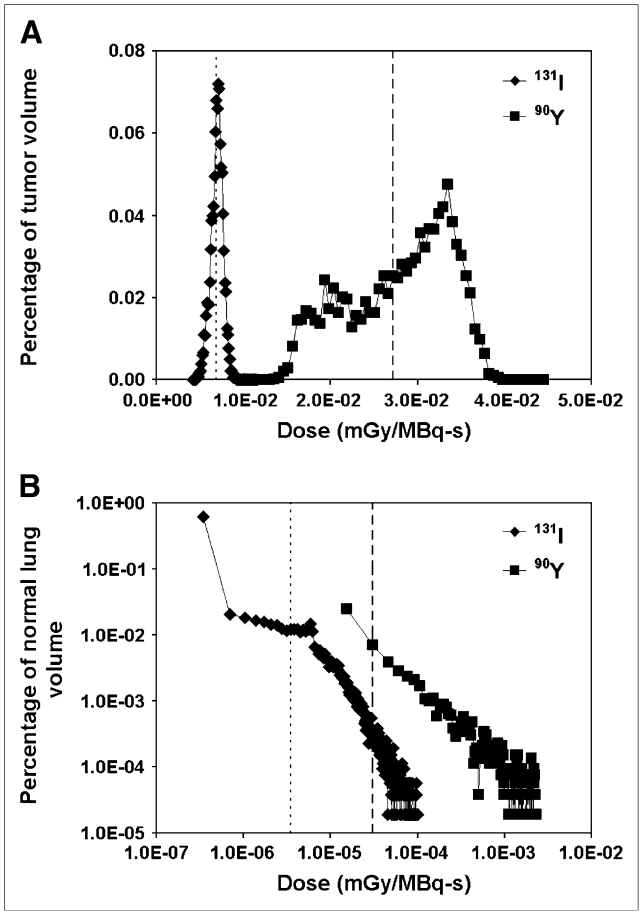

FIGURE 4. Dose–volume histograms calculated voxel by voxel with Monte Carlo–based dosimetry for tumors (A) and normal lung tissues (B) using either ^{131}I or ^{90}Y as sources. Mean specific absorbed doses to tumors and normal lungs are also shown for ^{131}I (dotted line) and ^{90}Y (dashed line).

higher-energy electrons, ^{90}Y delivers a greater average absorbed dose to tumors per disintegration than does ^{131}I. The average absorbed doses to 1.0-cm randomly positioned tumors were 2.72×10^{-2} and 6.86×10^{-3} mGy/MBq-s for ^{90}Y and ^{131}I, respectively. The dose–volume histograms, however, revealed a wider dose distribution for ^{90}Y relative to that for ^{131}I: The minimum absorbed doses for ^{90}Y and ^{131}I were 54.1% less and 33.3% less, respectively, than the respective mean values. Such a distribution will lead to tumor underdosing by ^{90}Y when the average tumor absorbed dose from ^{131}I matches that of ^{90}Y. Although absorbed dose in every voxel of ^{90}Y is larger than that of ^{131}I, this is counterbalanced by toxicity constraints. Therefore, the administered activity of ^{90}Y is usually smaller than that of ^{131}I. The dose–volume histogram for normal-lung volume is shown in Figure 4B. The average absorbed doses to the lungs were 3.06×10^{-5} and 3.45×10^{-6} mGy/MBq-s for ^{90}Y and ^{131}I, respectively. The maximum single-voxel doses reached 9.43×10^{-3} and 1.94×10^{-4} mGy/MBq-s, respectively. ^{90}Y and ^{131}I also have distinctive dose distributions in normal lungs. Because ^{90}Y emits only electrons, the normal-lung volume it can irradiate is limited, with about 7% of the lung receiving a radiation dose greater than 1.28×10^{-9} mGy/MBq-s when a tumor of radius 1.0 cm is the single source. For ^{131}I, however, every single voxel (100%) of normal-lung volume had significant energy deposited in it, mainly from the ^{131}I photons. As a result, lung voxels that do receive energy from ^{90}Y have much higher doses than the corresponding mean lung dose, whereas the dose distribution from ^{131}I is more uniform than that from ^{90}Y and the absorbed dose to a given normal-lung voxel is closer to the mean lung dose. This is demonstrated by the fact that for ^{90}Y, the maximum single-voxel dose was 3.1 times higher than the mean dose, and for ^{131}I, the maximum single-voxel dose was 55.4% higher than the mean dose.

The effect of surface distribution versus random distribution of tumor nodules was examined in terms of the absorbed dose ratio to normal lungs. Calculations were performed for both ^{131}I and ^{90}Y (Figs. 5A and B). The results showed that larger tumors tended to result in a relatively lower lung dose when they were located on the surface. For instance, with a tumor burden of about 60 g (about 6% of lung mass) in the lungs, the ^{131}I absorbed dose ratio from surface tumors to randomly positioned tumors decreased from 0.77 for tumors with radii of 0.2 cm to 0.54 for tumors with radii of 2.0 cm. The reduction in normal-lung absorbed dose for lung-surface tumors with larger radii occurred because the tumor tissue was farther from the lung surface, resulting in less dose delivered to the lung tissues. The decrease in normal-lung absorbed dose leads to an improved therapeutic efficacy for both ^{90}Y and ^{131}I. However, this improvement is more evident for ^{90}Y than for ^{131}I, because photons from ^{131}I make the lung dose less sensitive to variations in source positions. As shown in Figure 5C, the therapeutic efficacy of ^{131}I is still higher than that of ^{90}Y: For tumors with a radius of 0.2 cm, the maximum therapeutic efficacy ratio for ^{131}I to ^{90}Y decreased from 6.0 when the tumors were uniformly distributed in the lungs (Fig. 3C) to 5.3 when the tumors were on the lung surface.

DISCUSSION

Both ^{90}Y-ibritumomab tiuxetan and ^{131}I-tositumomab have been approved for treating relapsed or refractory low-grade follicular NHL and have shown similar overall objective responses. The choice of radioimmunoconjugates is of great interest for NHL patients at various stages of disease and with different tumor burdens and tumor nodule sizes. Pulmonary involvement in NHL is common clinically. In this work, we used Monte Carlo–based dosimetry to compare the efficacies of ^{90}Y-ibritumomab tiuxetan and ^{131}I-tositumomab, based purely on the emission properties of ^{90}Y and ^{131}I, in treating lung metastases in NHL patients. The absorbed dose to normal lung parenchyma served as the basis for comparison.

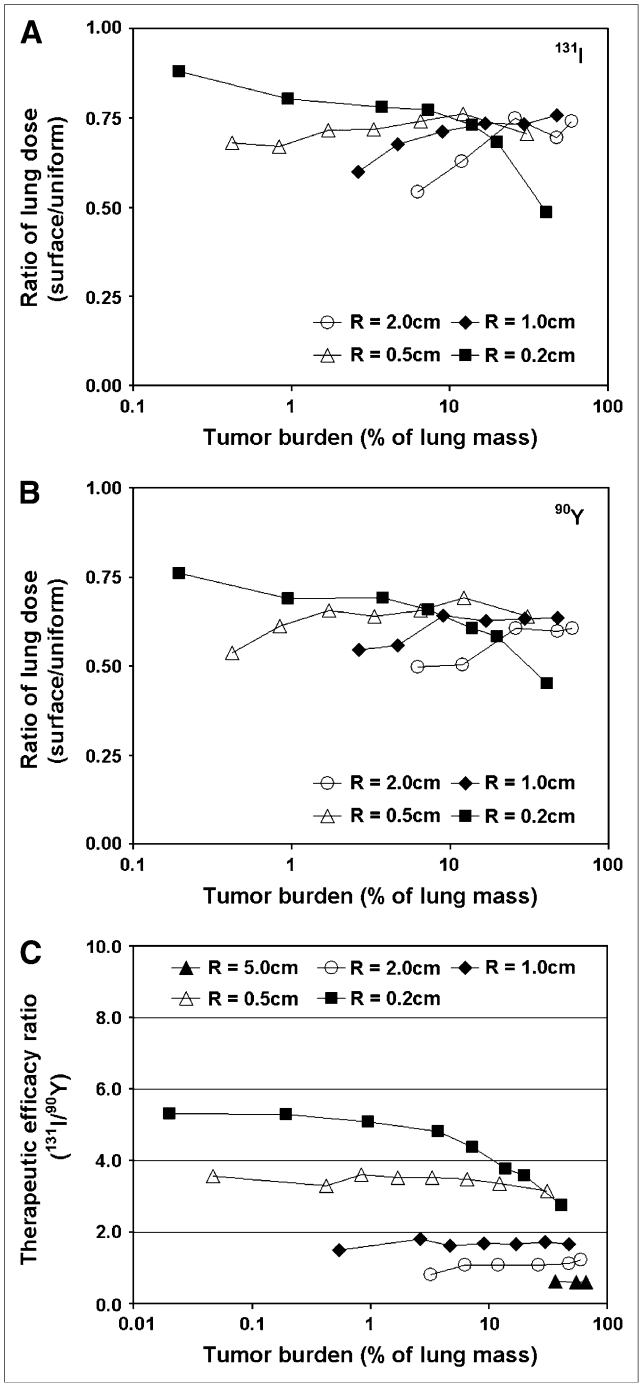

FIGURE 5. (A and B) Ratios of specific absorbed doses by ^{131}I (A) and ^{90}Y (B) to normal lungs when tumors were uniformly distributed in lungs or on lung surface. (C) Therapeutic efficacy ratio of ^{131}I to ^{90}Y. Tumor radii are from 0.2 to 2.0 cm.

The ^{131}I-based radioimmunoconjugate showed substantially better therapeutic efficacy than the ^{90}Y-labeled radioantibody when targeting smaller tumors (radius $<$ 2.0 cm) at a low total tumor burden. For larger tumors (radius $>$ 2.0 cm), ^{90}Y-labeled radioantibody showed increasingly better therapeutic efficacy. These findings were obtained with the assumption that both radiolabeled antibodies had identical targeting and pharmacokinetic properties. This approach made it possible to evaluate the impact of differences in their emission properties, all other things being equal. The pharmacokinetics could, however, greatly affect the limiting toxic doses and, thereby, the clinically achievable therapeutic efficacy. ^{131}I-Tositumomab has a more varied clearance among patients and therefore required pretreatment patient-specific dosimetry analysis (*3,22*). In a myeloablative setting, the lungs have been reported to be the dose-limiting organ for these patients, especially if there is pulmonary involvement. In such cases, the amount administered for therapy will be driven by the absorbed dose expected in the lungs. Assuming a maximum tolerated dose to the lungs, the ratio of activity retention between tumor and lung becomes the critical parameter in determining therapeutic efficacy. For whole-antibody–based radioimmunotherapy, the ratio of tumor to normal tissue is usually between 1.0 and 2.0, depending on the type of cancer being targeted (*23*). A past study has also reported a tumor-to-lung absorbed dose ratio of 1.5 using myeloablative doses of ^{131}I-tositumomab and stem cell transfer (*15*). In this study, we assumed, under the ideal situation, that activity was distributed only within the tumors. Including activity within the normal lungs would certainly lower the therapeutic efficacy for both ^{90}Y and ^{131}I. Given the high-energy β-emissions of ^{90}Y, however, it may be expected that the reduction would be greater for ^{90}Y than for ^{131}I.

The model-derived results provided here, however, neglect several potentially important factors that might affect response and toxicity. A particularly important one is dose rate (*24*). With a half-life of 64 h, a greater dose-rate effect may be expected from ^{90}Y than from ^{131}I, which has a 192.5-h half-life. The repair rate of normal lung parenchymal cells versus NHL tumor cells and the growth rate of the tumor will affect the degree to which dose rate is important Thus, the ability of normal lung tissue to recover from radiation damage, and the growth of specific NHL tumors that can be controlled by dose rate, need to be determined (*24*).

Although ^{90}Y has been predicted to be less effective in smaller tumors (radius $<$ 2.0 cm), this prediction was based on the assumption that activity is uniformly distributed in the whole tumor volume. This prediction is not, however, realistic, because tumors with a diameter larger than 2.0 cm may demonstrate nonuniform uptake of the radiolabeled antibody. Under such circumstances, a ^{90}Y-labeled radioantibody may have a better therapeutic efficacy because of the cross-fire effects from its more energetic electrons. Correspondingly, the dose distribution on the dose–volume histogram may be better for ^{90}Y than for ^{131}I. Clinically, NHL tumors with diameters larger than 1.0 cm may show better responses with ^{90}Y-ibritumomab tiuxetan (*16*).

Radioiodine-labeled antibody is internalized and catabolized by tumor cells to release iodotyrosine, which accumulates rapidly in the thyroid and stomach. Such antibody deiodination will not only increase thyroid dose but also

directly affect retention of radioiodine at the tumor site. Tumor doses may therefore be smaller for ^{131}I-labeled antibody than for radionuclides using stable metal chelates that achieve higher tumor retention. Normal-lung dose, which is part of therapeutic efficacy, will also decrease because of dehalogenation. Accurate dose estimation requires awareness of the dehalogenation kinetics from both tumors and normal lungs. Improved iodine labeling with residualizing peptide helps to enhance radioiodine retention in tumors and the therapeutic efficacy of ^{131}I-labeled radioantibodies (*25*).

Several animal studies have compared the therapeutic efficacies of ^{90}Y- and ^{131}I-labeled antibodies. In most subcutaneous xenograft models (including a lung carcinoma model), ^{90}Y appears to have superior therapeutic efficacy over ^{131}I (*26–30*), whereas in peritoneal (*31*) and lung metastasis (*32*) models, ^{131}I has resulted in better tumor responses. These findings are consistent with the results of this study and with the conclusion that ^{131}I is more suitable than ^{90}Y for treatment of small lung metastases at a low tumor burden.

CONCLUSION

Monte Carlo–based dosimetry was performed to compare the therapeutic potentials of ^{90}Y- and ^{131}I-labeled antibodies in targeting lung metastases in NHL patients. Therapeutic efficacy was better for ^{131}I-labeled antibody than for ^{90}Y-labeled antibody for smaller tumors with radii less than 2.0 cm and at lower tumor burdens. The comparison considered only the emission properties of the 2 radionuclides. The impact of differences in pharmacokinetics, dose-rate effects, nonuniform activity distribution, and radioimmunoconjugate stability was discussed.

ACKNOWLEDGMENTS

This work was supported, in part, by grant R01CA116477 from the National Institutes of Health, grant DE-FG02-05ER63967 from the Department of Energy, and grant BC044176 from the Department of Defense (a Multidisciplinary Postdoctoral Fellowship to one of the authors).

REFERENCES

1. Berkman N, Breuer R, Kramer MR, Polliack A. Pulmonary involvement in lymphoma. *Leuk Lymphoma.* 1996;20:229–237.
2. Maturen KE, Blane CE, Strouse PJ, Fitzgerald JT. Pulmonary involvement in pediatric lymphoma. *Pediatr Radiol.* 2004;34:120–124.
3. Juweid ME. Radioimmunotherapy of B-cell non-Hodgkin's lymphoma: from clinical trials to clinical practice. *J Nucl Med.* 2002;43:1507–1529.
4. Fisher RI, Kaminski MS, Wahl RL, et al. Tositumomab and iodine-131 tositumomab produces durable complete remissions in a subset of heavily pretreated patients with low-grade and transformed non-Hodgkin's lymphomas. *J Clin Oncol.* 2005;23:7565–7573.
5. Witzig TE, Flinn IW, Gordon LI, et al. Treatment with ibritumomab tiuxetan radioimmunotherapy in patients with rituximab-refractory follicular non-Hodgkin's lymphoma. *J Clin Oncol.* 2002;20:3262–3269.
6. Witzig TE, Gordon LI, Cabanillas F, et al. Randomized controlled trial of yttrium-90-labeled ibritumomab tiuxetan radioimmunotherapy versus rituximab immunotherapy for patients with relapsed or refractory low-grade, follicular, or transformed B-cell non-Hodgkin's lymphoma. *J Clin Oncol.* 2002;20:2453–2463.
7. Vose JM, Wahl RL, Saleh M, et al. Multicenter phase II study of iodine-131 tositumomab for chemotherapy-relapsed/refractory low-grade and transformed low-grade B-cell non-Hodgkin's lymphomas. *J Clin Oncol.* 2000;18:1316–1323.
8. Kaminski MS, Tuck M, Estes J, et al. ^{131}I-tositumomab therapy as initial treatment for follicular lymphoma. *N Engl J Med.* 2005;352:441–449.
9. Kaminski MS, Estes J, Zasadny KR, et al. Radioimmunotherapy with iodine (131)I tositumomab for relapsed or refractory B-cell non-Hodgkin lymphoma: updated results and long-term follow-up of the University of Michigan experience. *Blood.* 2000;96:1259–1266.
10. Press OW, Eary JF, Gooley T, et al. A phase I/II trial of iodine-131-tositumomab (anti-CD20), etoposide, cyclophosphamide, and autologous stem cell transplantation for relapsed B-cell lymphomas. *Blood.* 2000;96:2934–2942.
11. Press OW, Eary JF, Appelbaum FR, et al. Radiolabeled-antibody therapy of B-cell lymphoma with autologous bone marrow support. *N Engl J Med.* 1993; 329:1219–1224.
12. Gopal AK, Gooley TA, Maloney DG, et al. High-dose radioimmunotherapy versus conventional high-dose therapy and autologous hematopoietic stem cell transplantation for relapsed follicular non-Hodgkin lymphoma: a multivariable cohort analysis. *Blood.* 2003;102:2351–2357.
13. Winter JN, Inwards D, Erwin W, et al. Zevalin dose escalation followed by high-dose BEAM and autologous peripheral blood progenitor cell (PBPC) transplant in non-Hodgkin's lymphoma: early outcome results [abstract]. *Blood.* 2002; 100(suppl 1):411a.
14. Nademanee A, Molina A, Forman SJ. A phase I/II trial of high-dose radioimmunotherapy (RIT) with Zevalin in combination with high-dose etoposide (VP-16) and cyclophosphamide (CY) followed by autologous stem cell transplant (ASCT) in patients with poor-risk or relapsed B-cell non-Hodgkin's lymphoma (NHL) [abstract]. *Blood.* 2002;100(suppl 1):182a.
15. Liu SY, Eary JF, Petersdorf SH, et al. Follow-up of relapsed B-cell lymphoma patients treated with iodine-131-labeled anti-CD20 antibody and autologous stem-cell rescue. *J Clin Oncol.* 1998;16:3270–3278.
16. Silverman DH, Delpassand ES, Torabi F, Goy A, McLaughlin P, Murray JL. Radiolabeled antibody therapy in non-Hodgkins lymphoma: radiation protection, isotope comparisons and quality of life issues. *Cancer Treat Rev.* 2004;30: 165–172.
17. Song H, He B, Prideaux A, et al. Lung dosimetry for radioiodine treatment planning in the case of diffuse lung metastases. *J Nucl Med.* 2006;47:1985–1994.
18. Cristy M, Eckerman KF. *Specific Absorbed Fractions of Energy at Various Ages for Internal Photon Sources.* Oak Ridge, TN: Oak Ridge National Laboratory; 1987:25–26. ORNL/TM-8381.
19. Yoriyaz H, dos Santos A, Stabin MG, Cabezas R. Absorbed fractions in a voxel-based phantom calculated with the MCNP-4B code. *Med Phys.* 2000;27:1555–1562.
20. Audi G, Wapstra AH. Masses: Q-values and nucleon separation energies—the 1995 update to the atomic mass evaluation. *Nucl Phys A.* 1995;595:409–480.
21. Stabin MG, Sparks RB, Crowe E. OLINDA/EXM: the second-generation personal computer software for internal dose assessment in nuclear medicine. *J Nucl Med.* 2005;46:1023–1027.
22. Wahl RL. Tositumomab and ^{131}I therapy in non-Hodgkin's lymphoma. *J Nucl Med.* 2005;46(suppl 1):128S–140S.
23. Norrgren K, Strand SE, Nilsson R, Lindgren L, Sjogren HO. A general, extracorporeal immunoadsorption method to increase the tumor-to-normal tissue ratio in radioimmunoimaging and radioimmunotherapy. *J Nucl Med.* 1993;34: 448–454.
24. Dale RG. Dose-rate effects in targeted radiotherapy. *Phys Med Biol.* 1996;41: 1871–1884.
25. Stein R, Govindan SV, Mattes MJ, et al. Improved iodine radiolabels for monoclonal antibody therapy. *Cancer Res.* 2003;63:111–118.
26. Stein R, Chen S, Haim S, Goldenberg DM. Advantage of yttrium-90-labeled over iodine-131-labeled monoclonal antibodies in the treatment of a human lung carcinoma xenograft. *Cancer.* 1997;80(suppl 12):2636–2641.
27. Cardillo TM, Ying Z, Gold DV. Therapeutic advantage of (90)yttrium- versus (131)iodine-labeled PAM4 antibody in experimental pancreatic cancer. *Clin Cancer Res.* 2001;7:3186–3192.
28. Vallabhajosula S, Smith-Jones PM, Navarro V, Goldsmith SJ, Bander NH. Radioimmunotherapy of prostate cancer in human xenografts using monoclonal antibodies specific to prostate specific membrane antigen (PSMA): studies in nude mice. *Prostate.* 2004;58:145–155.

29. Brouwers AH, van Eerd JE, Frielink C, et al. Optimization of radioimmunotherapy of renal cell carcinoma: labeling of monoclonal antibody cG250 with ^{131}I, ^{90}Y, ^{177}Lu, or ^{186}Re. *J Nucl Med.* 2004;45:327–337.
30. Stein R, Govindan SV, Chen S, et al. Radioimmunotherapy of a human lung cancer xenograft with monoclonal antibody RS7: evaluation of ^{177}Lu and comparison of its efficacy with that of ^{90}Y and residualizing ^{131}I. *J Nucl Med.* 2001;42:967–974.
31. Koppe MJ, Bleichrodt RP, Soede AC, et al. Biodistribution and therapeutic efficacy of $^{125/131}$I-, ^{186}Re-, $^{88/90}$Y-, or ^{177}Lu-labeled monoclonal antibody MN-14 to carcinoembryonic antigen in mice with small peritoneal metastases of colorectal origin. *J Nucl Med.* 2004;45:1224–1232.
32. Sharkey RM, Blumenthal RD, Behr TM, et al. Selection of radioimmunoconjugates for the therapy of well-established or micrometastatic colon carcinoma. *Int J Cancer.* 1997;72:477–485.